Annu. Rev. Biophys. Biomol. Struct. 1998. 27:447–74

ON THE CHARACTERISTICS OF FUNCTIONAL MAGNETIC RESONANCE IMAGING OF THE BRAIN

S. Ogawa
Biological Computation Research, Bell Laboratories, Lucent Technologies, Murray Hill, New Jersey 07974; e-mail: so@physics.bell-labs.com

R. S. Menon
Laboratory for Functional Magnetic Resonance Research, The John P. Robarts Research Institute, London, Ontario, Canada N6A 5K8;
e-mail: rmenon@irus.rri.uwo.ca

S.-G. Kim and K. Ugurbil
Center for Magnetic Resonance Research, Department of Radiology, University of Minnesota Medical School, Minneapolis, Minnesota 55455;
e-mail: kim@geronimo.drad.umn.edu; kamil@geronimo.drad.umn.edu

KEY WORDS: functional activation, hemodynamics, metabolic load, BOLD, perfusion

ABSTRACT

In this review we discuss various recent topics that characterize functional magnetic resonance imaging (fMRI). These topics include a brief description of MRI image acquisition, how to cope with noise or signal fluctuation, the basis of fMRI signal changes, and the relation of MRI signal to neuronal events. Several observations of fMRI that show good correlation to the neurofunction are referred to. Temporal characteristics of fMRI signals and examples of how the feature of real time measurement is utilized are then described. The question of spatial resolution of fMRI, which must be dictated by the vascular structure serving the functional system, is discussed based on various fMRI observations. Finally, the advantage of fMRI mapping is shown in a few examples. Reviewing the vast number of recent fMRI application that have now been reported is beyond the scope of this article.

1056-8700/98/0610-0447$08.00

CONTENTS

INTRODUCTION

In the years since its introduction in 1992 (4, 58, 75), functional magnetic resonance imaging (fMRI) of the human brain has been well received as a noninvasive modality for studying human brain function and has rapidly become probably the widest-used method in investigating human brain function. The method is based on MRI signal changes due to hemodynamic and metabolic responses at the sites of neuronal activation induced by external and internal stimuli to the brain. Using this methodology, it is possible to construct whole brain activation maps for sensory and mental functions with high spatial resolution.

The most important role of fMRI in investigating human brain function arises from the fact that brain function is spatially segmented and compartmentalized. This functional specialization can be defined and mapped by fMRI utilizing secondary hemodynamic and metabolic responses to alterations in neuronal activity; in this sense, it is similar to positron emission tomography (PET) (78) where the most common approach for detecting brain activation is to measure regional cerebral blood flow (rCBF) by O^{15} water injection (97). An important additional feature of fMRI is its capability to follow signal changes in real time, even though the temporal (67) as well as spatial resolution (69) of fMRI is dictated by the characteristics of the hemodynamic response. While the time-constants of electrical activity of neuronal systems are shorter than some hundreds of msec, the hemodynamic response time is characterized by several seconds. Modalities such as EEG (electroencephalography) and MEG (magnetic encephalography) that can measure electrical and magnetic responses of the brain to evoking stimuli, on the other hand, encounter difficulties in accurately locating the sites of activation. Although the response time is on the order of seconds, fMRI can still take advantage of real-time data acquisition

and follow the time course of the signal change associated with mental activity that can evolve over seconds for particular cognitive tasks or specially designed paradigms. This is difficult to achieve in PET experiments.

Another modality of studying brain function—optical measurements of so-called "intrinsic signals" in visible wave length (63) to near infrared regions (50, 62, 96)—is also based on the hemodynamic and the metabolic responses. The chromophore monitored in these studies is mostly hemoglobin and the signal characteristics are very similar to those of fMRI.

The emergence of fMRI methodology is fundamentally based on the fortuitous presence of an endogenous contrast agent, paramagnetic deoxyhemoglobin, circulating in the brain and the tight coupling between neuronal activation and hemodynamic/metabolic responses. In addition, however, the rapidly developing MRI technology, largely driven by clinical applications and needs, has been a crucial factor that has made fMRI possible. This noninvasive technology has evolved to a point where relatively small regional signal changes can be detected and imaged over the whole brain with high reliability in localizing the sites of signal changes, and thus the sites of increased neuronal activity. There are already several published articles reviewing this rapidly growing field (17, 25, 55, 85). In this article, we discuss topics that characterize this modality and we focus mainly on our experiences.

METHOD

In fMRI, a large number of images—tens to several hundreds—are measured consecutively in a single experiment lasting anywhere from a few minutes to a quarter of an hour. The collected data are a time series of signal intensity from small volume elements or "voxels" covering regions of interest or the whole brain. During the data acquisition period, inputs for brain activation are presented to the subject in the magnet at appropriate periods. The input can be sensory stimulation, sensory input–guided cognitive tasks, subject-initiated mental activity, or even spontaneous brain activity the subject may not be aware of. Images taken during the absence of these inputs are used as a control. Image signals responding to the input are then compared with the control image signal (3).

It is preferable to image the whole brain simultaneously so that all the relevant activation patterns can be captured at once. Therefore, ultrafast imaging techniques, which may require extra MRI hardware, are indispensable. With echoplanar imaging (EPI) (89) or spiral k-space scan imaging (65), the magnetization induced from a slice in the brain by a single excitation can be measured at 64×64 2-D complex datapoints in as short as 30 msec to produce one image. In this acquisition time, the brain is virtually standing still. Within a few seconds, the whole brain area can be covered and the same image acquisition

sequence is repeated until the desired time series data are collected. Progress has been made to deal with some difficulties such as image distortion and signal losses in areas with severe phase dispersion (especially at high magnetic fields) in these fast imaging methods (43, 47, 103). Because there is a limit in the available time to measure the magnetization in the single-shot acquisition owing to the T_2^* signal decay, the in-plane spatial resolution is limited to a few mm. For higher spatial resolution, image acquisition is segmented to cover larger numbers of k-space data points in separate spin excitations. The FLASH (fast low-angle shot) imaging method, much slower in imaging, can acquire higher resolution fMRI images (31) at the expense of time.

Signal changes in fMRI are small and are typically only 1-to-several percent of the average image signal intensity. The signal change is larger at higher static fields. In a well-controlled comparison of signal activation by visual simulation with FLASH measurements at three field strengths, the fractional signal change in cortical gray matter was found to increase as 1.6 power of the static field (36). Although the instrumental noise in modern MRI instruments is getting below 1% peak-to-peak as measured in a phantom, the signal fluctuation in fMRI images of the brain is much larger. Even when head-motion is minimized by restraining the head, there are signal fluctuations of physiological origin. Cardiac and respiratory motions are the most notable ones. Even with fast imaging, the interimage signal fluctuation is substantial and induces signal alterations that exceed a few percent. When physiological signals are collected concurrently during MRI measurements, some retrospective signal correction can remove the signal fluctuation (44) to a useful degree. When MRI image acquisition is carried out faster, so that the Nyquist frequency is higher than the heart rate and therefore the respiration rate, the physiological fluctuations can be visualized in the power spectrum of the time series data (7, 70, 98). Such physiological oscillations present in the time series can be filtered out by postprocessing (5, 7, 70).

In the postprocessing of MRI data to extract functionally relevant signals, averaging over adjacent voxels with activated signals and also averaging in time are implicitly performed in various statistical analyses to generate activation maps (3, 33, 90, 101). All activation maps represent signal changes above a threshold. How to select this threshold in the statistical analysis is controversial, considering that the noise in MRI data is obviously not white as mentioned above. One way to improve confidence in selecting the threshold is to make the same experiment without the input task and to select the threshold on the basis of the dry run (70).

Choosing appropriate paradigms for fMRI experiments is probably the most important part of the experiment. Here, neuroscientists, neurologists, and psychologists play crucial roles, because it is important to clarify which elementary

neural substrates are involved in a given task. Although the MRI environment is not so friendly and there are limitations in implementing some tasks, one advantage of fMRI is that a few tasks in a paradigm can be nested with the control state and can easily be modified. An example where this feature was fully utilized is the mapping of the visual system in the human brain, where the input stimulus was varied in the visual field (space) with time continuously to activate the corresponding visual areas (26, 83).

FMRI SIGNAL

MRI Signal Response to Brain Function

Any direct effect of the electrical activity of neurons on water proton MRI has not been observed. There are extracranial magnetic fields generated by some concerted neuronal activities in localized areas of the brain. They are detected and used for functional studies by MEG. However, their magnetic effect at the site of the activity appears very small for water spins to sense and has eluded detection by MRI.

When there are moving water spins, they can be detected by MRI. The major part of the moving spins detected in the brain arise from blood water flowing in arteries and veins (angiography). Recently, however, blood-water perfusion in the capillary bed has been imaged to yield maps of rCBF and rCBF alteration coupled to functional activation. Water diffusion in the brain tissue has been measured to study the brain cell swelling in cases such as stroke (95) and spreading depression (61). If there is appreciable water movement into or out of brain cells associated with functional activation, some change in the apparent water diffusion constant could be expected. This effect seems to have been detected, but for some reason the response time is very slow in minutes (106).

In optical experiments, changes in light reflection or scattering by brain activation have been reported (38, 63) as a fast-response phenomenon associated with neuronal activation. There have been no reports of detectable MRI changes related to these phenomena except a small but fast decaying signal in functional MR spectroscopy of water (42).

Because deoxyhemoglobin in red blood cells is paramagnetic, there are susceptibility-induced field variations in and around blood vessels, and water spins sense the local field distortion. The hemodynamic and metabolic changes associated with brain functional activation influence the deoxyhemoglobin content in the tissue, and the induced signal change in MRI can represent the functional activation. This deoxyhemoglobin effect has been called the blood oxygenation level dependent (BOLD) effect (73).

Regional hemodynamics and metabolic load are tightly coupled to the regional neuroactivation and therefore BOLD as well as perfusion measurements

are the main part of fMRI. The MRI signal of an image voxel is a sum of the water signals from components such as tissue, blood, or bulk cerebrospinal fluid (CSF), and has T_1^* dependent (flow sensitive) and T_2^* dependent parts as expressed in Equation 1 for one component (labeled as x).

$$S_x = v_x \cdot S_{0x}\left(T_{1x}^*\right) \cdot A_x\left(T_{2x}^*\right) \cdot \exp(i\phi_x) \quad (1)$$

where v_x is the volume fraction of the component and A is the attenuation factor due to the T_2^* decay ($1/T_2^* = R_2^*$) during the echo time (t_e) of the signal acquisition [$\sim \exp(-t_e/T_2^*)$]. As a part of $1/T_2^*$ signal decay, the blood susceptibility effect contributes to the $1/T_2^*$ decay and $A = A_0 \cdot A_{sus}$. The residual phase ϕ_x of the signal, if any, mostly comes from a small off-resonance frequency of the component, including the field shift by red cells with deoxyhemoglobin. Signal changes occur when these relaxation parameters follow the hemodynamic and metabolic changes.

The total signal S is a sum of the contribution from the component S_x, $S = \Sigma S_x$. In usual fMRI analysis, the fractional signal change from control state is taken as a difference in the signal magnitude, $\Delta S/|S| = \Delta|S|/|S|$, instead of the phased difference $\Delta S/|S| = \Sigma \Delta S_x/|S|$ due to the phase instability of the signal which tends to increase noise more in the latter value. When the residual phases, ϕ_x's, are small, the two values of signal changes are essentially the same. When a vein occupies a large portion of an image voxel, the phase ϕ differs from the nearby voxels with tissue only. This has been used to generate a high-resolution venogram image (16, 60).

Inflow Effect and Perfusion

When signal acquisition is performed rapidly to cause T_1 saturation of the water signal (S_{0x} term in Equation 1 is reduced from 1), the extent of saturation is less in blood water because the fresh blood-water spins flow in from the neighboring region outside of the RF excitation. Thus, the relaxation rate is no longer determined by $1/T_1$ but by a faster rate defined as $1/T_1^*$, which contains the flow effect. This $1/T_1^*$ by flow is further enhanced by functional activation, especially at larger vessels where the flow velocity is high. Most of the signal activation with the inflow effect occurs in veins but not in arteries. In the latter, the flow is so fast (tens of cm/sec) that all blood-water content is replaced within the RF repetition. When a large vein shows activation by the inflow effect, it gets the fresh blood water from the neighboring area and not from the area in the observing image slice. This means that the corresponding neuroactivation sites are fairly away from the vein. Strategies in signal acquisition to avoid or to increase the inflow effect have been discussed in various papers (32, 35, 55, 56).

Recently, it has become possible to make quantitative measurements of the above inflow signal to capillary beds where blood water perfuses through the

tissue. The change in the perfusion signal by functional activation is an rCBF change and an important element of fMRI. Many methods aiming to make perfusion measurements use spin-tagging, by preinversion or presaturation of either inflowing spins (21, 23, 99) or the spins in the zone of observation (52, 58); in both cases, spins coming into the area of observation are then examined by comparing to data obtained with no tagging (52). The simplest and probably cleanest among these methods is the flow-sensitive alternating-inversion-recovery (FAIR) method (52, 53, 59). Here, spins in the observing slice are first inverted (local inversion), and after a period of about $T_1(1 \sim 2\,\text{sec})$ during which uninverted fresh blood water spins flow into the slice, sampling pulses are given to get the slice image. As a control to the local inversion recovery imaging, a global inversion of spins is made. In this case, the flow-in spins do not have any distinction from the local spins and take the same inversion recovery course as the latter. From the difference of the two cases, one can estimate the amount of blood flow into the voxel during the period of the "incubation." The inflow signal in capillary beds gets stronger, with an incubation time longer than the transit time of flowing blood from arterioles through capillaries to venules. The uninverted blood water spins following into the capillaries is not simply refilling the vascular space but exchanging with the tissue water (perfusion). The perfusion or the exchange of the water molecules between capillary and the surrounding tissue is a fast process (99) as compared with the "incubation" time of a second or two. When the blood flow gets very high, however, the exchange becomes incomplete (24, 99).

The estimated quantity from these perfusion measurements is essentially the CBF (ml of blood/gram of tissue/min) at each voxel in the image. Thus, these perfusion methods provide easily interpretable quantities for functional activation, namely the regional CBF change.

BOLD Effect

Blood water $1/T_2$ has been known to increase with blood deoxygenation because of the susceptibility effect from red cells (91). This susceptibility effect due to deoxyhemoglobin has also been observed in brain MR images (73). The enhancement of the apparent relaxation rate constant $1/T_2^*$ (in gradient echo images) occurs not only in the blood water but also in the tissue water around blood vessels. The BOLD effect changes with the physiological conditions of the brain under which the deoxyhemoglobin content varies (73). A temporal ischemic episode was followed by the $1/T_2^*$ change in time (94).

The signal attenuation, A_x in Equation 1, is caused by intravoxel dispersion of the signal phase ($\phi = \delta\omega \cdot t_e$) resulting from the local field ($\delta\omega$) induced by the red cell susceptibility. This is expressed by the voxel average of the water signal phase factor $\langle \exp(i\phi) \rangle_{\text{voxel}}$ in space and time (movement of water molecules).

The extent of this averaging, $\langle \exp(i\phi) \rangle_{voxel}$, differs among the water molecules in intra- and extravascular spaces of capillary and venule compartments as well as areas containing large veins (1, 8, 9, 28, 51, 74, 102). For the blood-water, the water exchange between red cells and plasma—where the susceptibility-induced fields differ—is an important process for the averaging (105). By spin echo data acquisition, the relaxation rate $1/T_2^*$ is smaller than the rate $1/T_2^*$ appears in gradient echo because of the refocusing effect of the phase inversion pulse in the former on the averaging. The susceptibility-dependent $1/T_2^*$ of the blood-water is much larger than that of the extravascular tissue-water, but the volume fraction v_b is small ($0.02 \sim 0.04$).

Song et al (88) showed that fMRI BOLD signals from the motor cortex during a finger-tapping task at 1.5 Tesla disappeared when a relatively small dipolar diffusion gradient (b-factor of 42 sec/mm^2) was applied during the signal acquisition. With this diffusion gradient, intravascular signals from non-capillary vessels with blood flow velocities of above several mm/sec would be dispersed out. This indicated that these fMRI signals were intra-vascular and mostly contributed by noncapillary vessels.

A further study at 1.5 Tesla (8) showed that two-thirds of fMRI signals in visual stimulation experiments were from moving spins and were lost with diffusion gradient of $b = 600$ sec/mm^2. These signals, acquired by asymmetric spin echo (165 msec echo time t_e for spin echo with 20 msec gradient echo contribution), were inside homogeneous gray matter regions without the presence of any obvious large vessels. At higher B_0 fields of 3 Tesla (87) and 4 Tesla, however, substantial fMRI signals in gradient echo acquisition persisted even with diffusion gradient of $b = 400$ sec/mm^2, showing that the extravascular contribution becomes more important at higher B_0 field.

When a voxel contains a large vein, the signal activation is very large (several to 20 percent). The signal change $\Delta S/S$ has contributions

$$\Delta(S_{0,blood} \cdot v_b \cdot A_{0,blood} \cdot A_{sus,blood})$$

from blood water as seen from Equation 1. It will be enhanced by a large blood volume fraction v_b in the voxel and high $S_{0,blood}$ resulting from inflow effect, if any. The anisotropic orientation dependence of the susceptibility effect is not averaged for a large vein. Therefore, $A_{sus,blood}$ itself can vary sharply with the oxygenation and similarly the extravascular contribution (72) also can be large.

In a venule compartment of gray matter, if a CBF increase of 60% raises the venous blood oxygenation Y from 0.6 to 0.75, the signal change contributed by the blood water, $\Delta(v_b \cdot A_{sus,blood})$, at 1.5 Tesla would be 0.8% with an echo time of 40 msec, taking the susceptibility dependent $1/T_2^*$ of the blood water at $Y = 0.7$ to be 11 sec^{-1} (8, 15). At higher B_0, the $1/T_2^*$ of the blood and also the sensitivity to the oxygenation increase, but the signal change does

not necessarily become larger, because at the basal physiological condition $A_{sus,blood}$ itself is diminishing strongly with t_e (more attenuated blood water signal). At 4 Tesla with the same hemodynamic condition as above and $1/T_2^*$ of 31 sec^{-1}, $\Delta(v_b \cdot A_{sus,blood})$ would be 0.7%. On the other hand, the extravascular contribution increases with B_0 field linearly or with a higher power up to 2.

The measurement of the BOLD effect is simple with gradient echo or spin echo imaging. However, the quantitative aspect of the signal change is not clear because it could be influenced by many unknown parameters of the vasculature and hemodynamics. The expression for the signal change appears to be not as simple as

$$\Delta S/S \sim \Delta\left(1/T_2^*\right) \cdot t_e \sim a \cdot t_e \cdot \Delta\{(1 - Y) \cdot v_b\},$$

predicted some time ago (72). Efforts are being made to calibrate BOLD signals empirically in terms of measurable hemodynamic and vascular parameters, $\Delta S/S = \text{func}(Y, \Delta Y, v_b, \Delta v_b)$, by using a hypercapnia condition that allows investigators to vary CBF, and therefore cerebral blood volume (CBV) (40) and blood oxygenation without changing the oxygen consumption rate (2, 20, 82). Although there may be some difference in vascular responses between the conditions of functional activation and hypercapnia, the latter is so far the only approach easily accessible for this calibration. An empirical fit such as

$$\Delta S/S = a(\Delta Y) + b(\Delta v_b/v_b) + c(\Delta Y)(\Delta v_b/v_b)$$

or in other functional forms of these parameters (20) has to be found for the quantitative analysis of the BOLD effect.

Physiological Connection of fMRI Signal

Fick's principle for arteriovenous oxygen balance relates oxygen extraction (or oxygen consumption) to CBF and venous blood oxygenation level (Y), and the latter is a relevant parameter to determine BOLD signal changes. Under normoxic conditions,

$$(oe) = CBF \cdot C_h \cdot (1 - Y),$$

where (oe) is the rate of oxygen extraction and C_h is the heme concentration in unit volume of blood. Oxygen extraction factor OEF (the fraction of oxygen extracted from arterial blood oxygen), an often used parameter, is

$$OEF = (oe)/(CBF \cdot C_h) = 1 - Y.$$

When there are changes in the metabolic load and hemodynamics, Equation 2 describes the changes in the above balance between the two steady states.

Assuming the hematocrit does not vary,

$$1 + \Delta(\mathrm{OEF})/\mathrm{OEF} = (1 + \Delta(\mathrm{oe})/(\mathrm{oe}))/(1 + \Delta\mathrm{CBF}/\mathrm{CBF})$$

$$= 1 - (\Delta \mathrm{Y})/(1 - \mathrm{Y}). \quad (2)$$

The knowledge of CBF increase and ΔY can lead to Δ(oe) estimate from the equation. If one can analyze the BOLD signal quantitatively to estimate ΔY, then CBF and BOLD measurements could lead to characterize the metabolic load associated with the functional neuroactivation (2, 20, 54).

If the hemodynamic response to neuronal activation proceeds without OEF change, $\Delta(\mathrm{OEF}) = 0$, or $\Delta(\mathrm{oe})/(\mathrm{oe}) = \Delta\mathrm{CBF}/\mathrm{CBF}$. With this complete coupling of ΔCBF/CBF to Δ(oe)/(oe), a BOLD signal will not show any appreciable positive increase in the presence of a CBF increase ($\Delta \mathrm{Y} = 0$ and $\Delta \mathrm{v_b} > 0$). With photic stimulation, ΔCBF/CBF ($\sim$50%) has been shown to far exceed Δ(oe)/(oe) ($\sim$5%) in the visual area in the human brain (29, 30). With these changes in Equation 2, then $\Delta(\mathrm{OEF})/(\mathrm{OEF}) - (\Delta \mathrm{Y})/(1 - \mathrm{Y})$ is -0.3. At $\mathrm{Y} \sim 0.6$ for the resting state, ΔY becomes 0.12 in this uncoupled hemodynamic change from the oxygen extraction change. Most fMRI (BOLD) signals observed in functional activation are positive and show very similar activation maps as CBF measurements by PET or perfusion measurements by MRI. The disparity of the CBF increase over (oe) increase is a common phenomenon in functional activation.

An early attempt to correlate BOLD and perfusion measurements with a visual stimulation paradigm is shown in Figure 1 (54). The two measurements (FAIR and BOLD) are alternately made in a time series of one experiment. The data are from a total of 29 measurements in 12 subjects and each point is a spatial average in the common ROI covering most of the primary visual cortical ribbon seen in a slice image. The average value of ΔCBF/CBF is 43%, consistent with previous PET measurements (30). There the points are scattered widely in CBF as well as BOLD signal percent changes even though the paradigm was the same for all subjects. There is a scant correlation that the CBF increase is accompanied with BOLD increase. One would argue that the comparison has to be made at a pixel-by-pixel level for the common activation sites in a single subject with a multitrial average to establish the quantitative relation between the two measurements.

Neuronal Activation and fMRI Signal

Although the quantitative aspect is still to be clarified, the BOLD signal has been shown to reflect neuronal events. The dependence of a BOLD response on the flashing frequency of red and black or black and white checkerboard stimulation is—as in the case of rCBF in the visual area—quite consistent with the known neuronal response to this stimulation (58). When the evoked

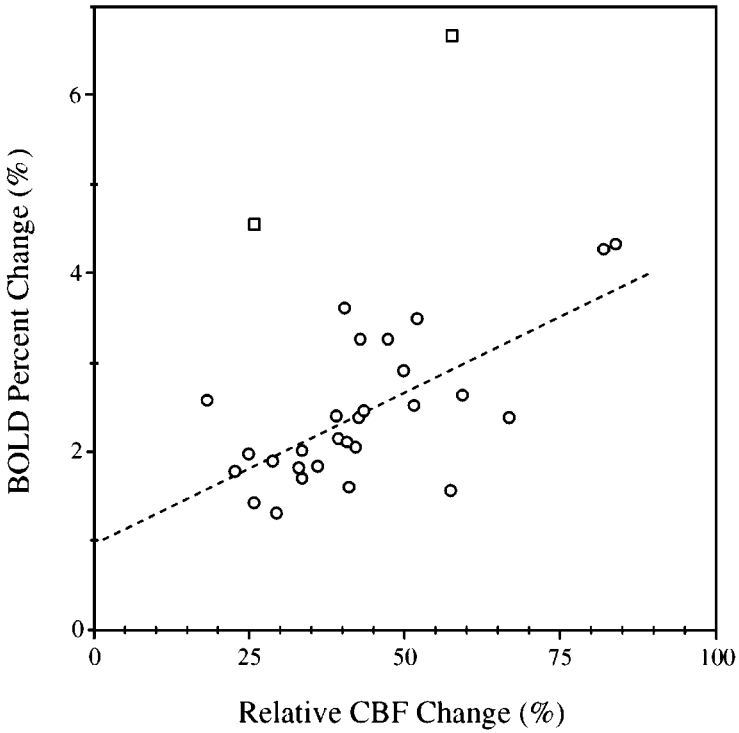

Figure 1 Relationship between BOLD and CBF changes during visual stimulation at a frequency of 8 Hz using goggles. BOLD with a gradient echo time of 30 msec and FAIR images were acquired at 4 Tesla in an alternative manner. A total of 29 measurements were performed in 12 subjects. The region of interest is the gray matter area in the primary visual cortex, chosen from anatomic images. To correlate CBF and BOLD changes, two points with the *square symbol* were not included. The best fitted line is that BOLD(%) $=$ 0.028*CBF(%) $+$ 1.3 (r2 $=$ 0.26).

potential induced by electrical stimulation at the frontal paws is monitored by an intracranial electrode in the sensorimotor area in the rat brain, the electrical activity peaks at the stimulating frequency of 3 Hz and decreases above that frequency. The corresponding BOLD signal also shows quite similar frequency dependence, indicating it is reflecting the neuronal events very well (41).

Figure 2 shows a comparison of fMRI responses to a motor task in human subjects (79) with electrophysiological measurements in a trained monkey (L Shen, GE Alexander, private communication) having a very similar motor task paradigm. Using a visual input, the subject was instructed how to move his right hand fingers in a finger sequence and told to refrain from executing

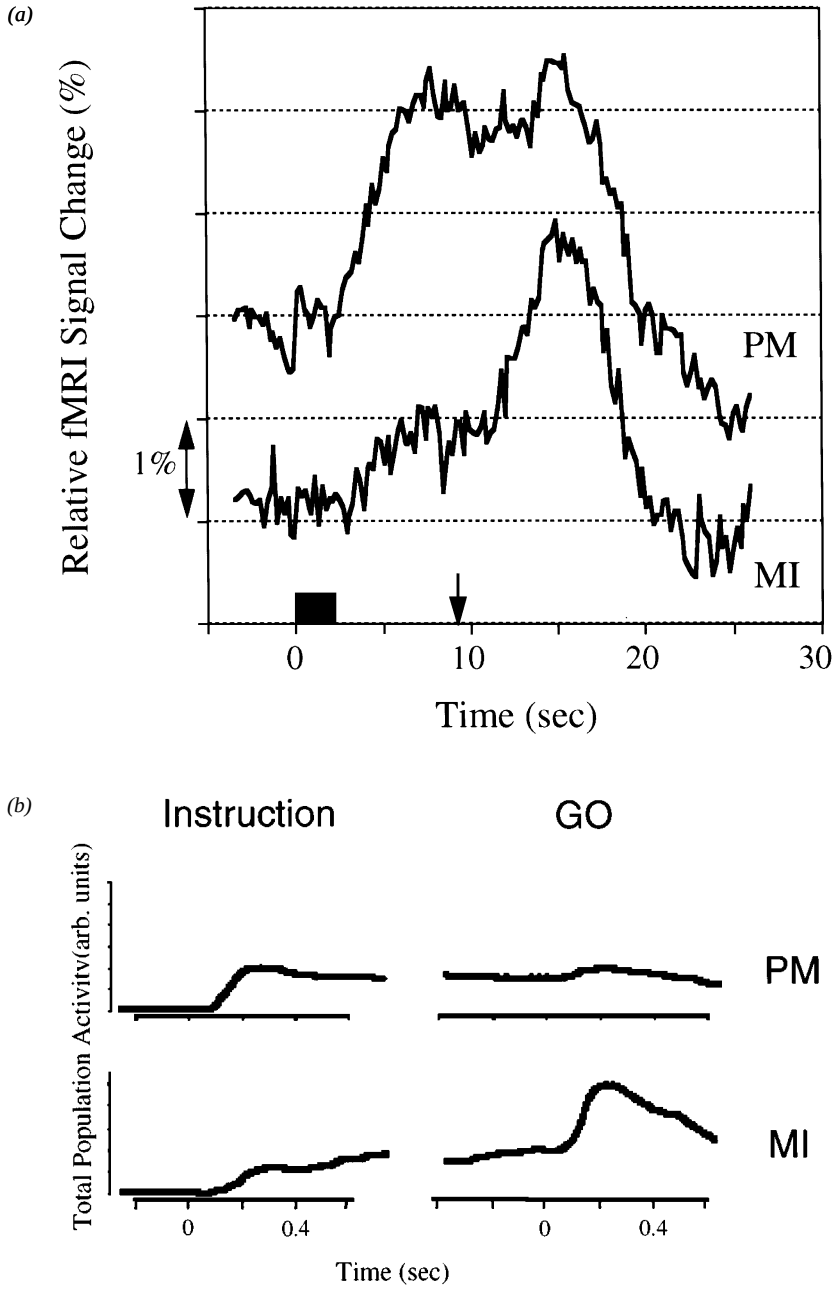
(a)
Relative fMRI Signal Change (%)
1%
PM
MI
0
10
20
30
Time (sec)
(b)
Instruction
GO
Total Population Activitv(arb. units)
PM
MI
0
0.4
0
0.4
Time (sec)

the task until a "GO" command appeared on the screen. The responses in the primary motor (M1) and premotor (PM) areas are shown in Figure 2*a*,*b* (80). In the M1 area, the signal increased slightly after visual instruction and much more after a GO cue in both human fMRI and monkey single-neuron recording studies. Further, in the PM, magnitudes of signal changes before and after the GO cue are similar in both studies. Although hemodynamic response is delayed and could be blurred, temporal patterns of fMRI and total population activity are extremely similar. The electrical activities in the plots (Figure 2*b*) are averages from single-electrode intracellular recordings at more than 100 of output neurons in each area and the activities occur as subsecond time scale events. It is interesting that the fMRI response pattern follows the population activity of the areas and not necessarily some peak activity of certain cells observable in the intracellular recording (L Shen, GE Alexander, private communication).

The aforedescribed observations support the validity of numerous BOLD-based functional maps of the human brain already acquired and indicate that these maps actually represent the sites of the brain activation of interest.

COUPLING OF HEMODYNAMICS AND METABOLISM TO NEURONAL EVENTS

Recently, Jueptner and Weiller (48) reviewed issues concerning the relationship of synaptic activity to rCBF and metabolic load. Most of relevant questions with respect to this problem can also be found in Raichle's earlier review (78). Many of these questions remain unanswered today.

Although the induced rCBF increase is a well recognized indicator for elevation of electrical activity, the mechanism of activation-related rCBF control is not yet established. There are many candidates for mediating the control, such as K^+, NO, adenosine, CO_2, direct electrical connection to vasculature, and so on. None of them has been shown to be the sole controlling factor, but several may be involved (100). It is not clear that CBF control is from the spike-generating neuronal cell bodies or from the neuropils (areas of synaptic

←

Figure 2 Dynamic BOLD-based fMRI signal changes in humans (*a*) and population activities in a trained monkey (*b*) during a delayed motor task. The primary motor area (*MI*) and premotor (*PM*) are shown. The task consists of instruction, delay, GO cue, and movements. Instruction is given visually for movements (shown as *box* in *A*; time = 0 at instruction in *a*), and subjects move after a GO cue (*arrow* in *a*; time = 0 at GO in *b*). The delay time between instruction and GO is 7 s for humans and 1.0–1.5 s for monkey studies, during which subjects are supposed not to move. In both studies, movements were monitored during performance of a task using electromyography. Because a delay time in *b* is randomized, averaging was performed to lock (time = 0) either the visual presentation (*left* time courses) or GO cue (*right*) (79, 84).

endings at dendrites) participating in the activation and consuming with oxidative metabolism most of the energy for the increased activity. In the high-resolution fMRI maps of whisker-barrel activation in the rat brain shown by Yang et al (104), the layer IV of the activated cortex appears as the major site of CBF increases. The layer in this cortical area is well vascularized and contains these barrels characterized by the high population of cytochrome oxidase (19). However, this does not necessarily indicate that the neuropil activity triggers the CBF increase. On the other hand, the intracellular recordings, from which Figure 2*b* is obtained, are from spiking neurons in the output-generating layer of the motor cortices. Because the temporal response patterns of the population activity in these neuronal cells and the fMRI are so much alike except in time scale (Figure 2*a* and 2*b*), they may suggest the possibility that the neuronal cells contributing to the population spiking have some role in triggering or sustaining the hemodynamic response.

The larger fractional CBF increase relative to the fractional oxygen consumption elevation with neuroactivation leads to the possibility that the elevated glucose use that occurs together with the increased CBF following heightened neuronal activity is quite anaerobic. Lactate production in visual areas during photic stimulation has been observed in fMR spectroscopy (77). Recently, a new scheme for the anaerobic glucose metabolism has been presented. Anaerobic glucose metabolism in astrocytes is promoted by the increased synaptic activity in the neuropil to take up excess released glutamate, which is the major transmitter in mammalian CNS (76, 93). Some portion of lactate produced is used oxidatively at the neurophil to support the energy demand.

In contrast to the anaerobic glucose use mentioned above, a highly oxidative cerebral metabolic rate of glucose ($CMR_{glucose}$) increase has been reported in C^{13} MR spectroscopy study of sensorimotor cortex activation in α-chloralose anaesthetized rats. Following the C^{13} labels from injected glucose to glutamate, the Yale group (46) has measured a significant and large increase in the tricarboxylic acid cycling rate that is linked directly to $CMR_{glucose}$ and also related to the recycling of transmitter glutamate. If this is the case, the uncoupling of CBF and oxidative metabolism has a different meaning from the one described above. The appearance of lactate has to be a temporary phenomenon and quantitatively not meaningful. In this scheme of metabolism, the activation-induced changes in CBF and $CMR_{glucose}$ will lose their strong linkage (37, 81). Buxton et al (12) have presented a model to make the disparity between oxygen extraction and CBF increases [$\Delta(oe)/(oe) \ll \Delta CBF/CBF$] consistent for a completely oxidative metabolism. There, the $CMRO_2$ increase dictates the CBF that is required to increase disproportionately in order to elevate the O_2 concentration gradient from the blood to the tissue. In this model, however, the increased "available" oxygen in the tissue observed with oxygen electrodes in

situ during sensory and motor activation in the human brain is not explained (78, 86).

TEMPORAL CHARACTERISTICS

Figure 3 shows temporal response patterns of tissue BOLD signal at 4 Tesla in the primary visual area during and following a series of brief photic stimuli of different durations (45).

All time courses display initial small signal decreases, or "dips," reaching their minimum (average 1.2%) within a few seconds after the onset of the stimuli, followed by much larger positive signal increases. After the termination of the stimuli, the signal decays in several seconds. The time up to ten seconds and the undershoot of the decay response depend on the length of the stimulation period. The initial dip as observed by Menon et al (67) is small and difficult to detect in a BOLD signal. It has been reported so far only in

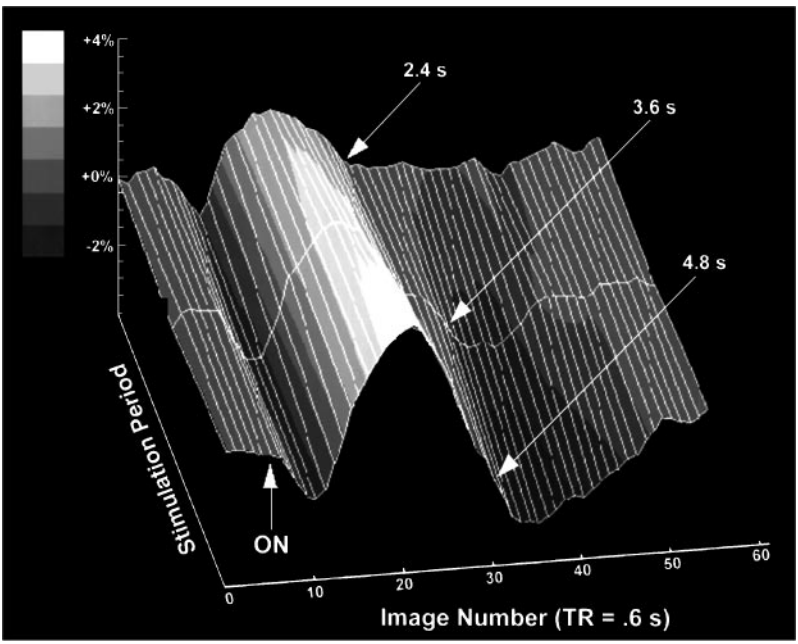

Figure 3 Time courses of fMRI response at 4 Tesla in a V1 region to brief visual stimulation. The three time courses correspond to stimulus duration (8 Hz flashing LED) of 2.4, 3.6, and 4.8 seconds. Four segmented EPI with TR/TE = 600/30 (msec) was used and retrospective physiological fluctuation correction was applied (45).

high-field measurements of photic stimulation (45, 66, 67). The negative dip has been attributed to an increase of the deoxyhemoglobin content in the tissue caused by the increase of the metabolic load as shown by optical imaging data (39) on an awake monkey. More recently, an optical imaging spectroscopy study of the cat brain by Malonek and Grinvald (63) showed that despite the increase of deoxyhemoglobin, oxyhemoglobin content did not change much. This indicates that in this early response period there is some blood-volume increase in addition to the decrease in the blood oxygenation. The fMRI signal decrease could be due to the extravascular $1/T_2^*$ contribution, which is more pronounced in high field as described before (13). The initial dip is presumably due to the increased metabolic load and should be well localized at the site of activation and free from the large-vessel contribution often seen in the later period. The subsequent increase in rCBF makes the area hyperoxygenated and the signal becomes positive ($1/T_2^*$ decrease owing to deoxyhemoglobin decrease) and large. In most cases, the activated signal levels last during the stimulation period. This signal increase in the period is usually used for functional mapping. As seen in Figure 3, after the termination of the photic stimulation, the signal stays up for some seconds and then decays. The "undershoot" in the decay time course, which is observable with longer duration of stimuli, is likely due to the unbalanced metabolic energetics yet to settle (the oxygen consumption rate is still elevated) or the slow return of the increased blood volume fraction (CBV) to the basal state. The latter delayed vascular response has been shown in animal models (64). It is interesting to note that this undershoot, which is slightly larger than the initial dip, has been observed relatively easily by 1.5 Tesla field measurements too. Since the major component of the signal change at 1.5 T appears to be the blood water signal, the vascular volume decrease in this recovery process should lead the signal from high to low. Therefore, the vascular recovery alone cannot explain the observed undershoot.

The temporal response of fMRI signals as mentioned above is dictated by the hemodynamic response of the vascular system and is slow with a time constant of many seconds. However, fMRI is a modality of real-time measurements and the period of the signal activation tracks the period of stimulation very well if the latter lasts long enough for fMRI detection. This tracking of activation extends to brain areas of cognitive functions. For studying cognitive function, a single run–single trial experiment is often highly desirable. As a recent trend, such single-trial activation studies have been drawing interest (11, 80), taking advantage of this real-time tracking feature. For example, Richter et al (80) have studied single-trial activation at parietal areas with a "mental rotation" task. The areas are known to be involved in spatial information processing. The subject is first shown a picture of a block assembly that spans a reasonably complicated space. Later, a similar block assembly in different view is shown

to the subject and the subject has to decide if the object is the same as the one first seen by mentally rotating the new object. When he/she reaches a decision, the subject presses an appropriate button to inform of the decision. The time required to reach the decision varies with the difficulty of the task. This reaction time (in many seconds) correlates extremely well with the period of the fMRI signal activation, indicating that the signal activation is following closely the on-going neuronal function. Similar results can be seen in Figure 2*a*, where behaviorally nonexplicit brain functions as well as explicit ones can be traced in the temporal response time course of fMRI.

Another type of temporal response pattern has been observed in hippocampus and cerebellar dentate nucleus (49) with a memory task. When a subject memorizes aurally given repeated words during a period of 50 s and then stops the effort of memorizing, the activation in these areas returns to the base line extremely slowly, taking one minute and a half to decay. In this period, the subject is not actively engaged in memorization. In auditory areas, the decay is immediate after the active task period. In Broca's area and Wernicke's area the decay is somewhat slow, with a decay time of 50 seconds. When a finger-tapping task is enforced during the slow decaying period of 90 s after the memorization task, the performance score of the original memory efforts deteriorates to an applicable degree. This observation of extra-slow retarded responses is unexpected and remains unexplained. Since the hippocampus is known to get easily sensitized for activation (81), some parts of memory activity (such as consolidation of memory) could last for some time without the subject's active participation.

When time-series data of fMRI are "denoised" (see Methods) and free from the contamination of irrelevant signal fluctuation, the data could reveal various types of spatiotemporal patterns; some are task-related and others may be spontaneous (70). MRI signals of resting human brain contain low-frequency oscillations at about 0.1 Hz. They are attributed to vasomotion, which is dependent on physiology but not necessarily on the electrical activity. Such vasomotion with several percent variation in CBF is known in experimental animals (71). It is interesting to note that a fairly early study of tissue oxygen in the human brain (18) showed a small fluctuation of O_2 level at about 0.1 Hz.

In denoised time-series data of the resting brain, Biswal et al (6, 7) has shown intra- and interhemispheric correlations among spontaneously varying signals of motor-related areas. They mapped the correlated areas to show a pattern of possible functional connectivity in those areas. Although it is yet to be shown that the origin of the correlation is neurophysiological, the observation is very exciting. This is a demonstration of the unique advantage of fMRI capable to gather spatiotemporal information of the brain function even without explicit input task to the subject.

SPATIAL RESOLUTION

There are various aspects to spatial resolution in fMRI. The signal activation can be seen at a large draining vein that may be several mm or more away from the activation site, local veins near the area of activation, and the tissue that contains capillaries and venules (32, 56, 69). These areas can be distinguished more or less by looking at the corresponding anatomical image at high resolution as well as the flow-sensitized image that depicts large vessels. Large veins often show large signal changes relative to tissue activation in gradient echo signal acquisition and therefore can be screened out from the activation map. As mentioned earlier, the fast-moving blood water signal from large vessels can be eliminated by imposing a weak bipolar diffusion gradient. In functional mapping by fMRI, the area of activation is often several mm or larger (a cluster of more than 2×2 pixels with 3 mm square pixel size). If one needs only the spatial resolution of these sizes, the mapping by tissue signals or even local vein signals serves the purpose.

Because the region served by the vasculature that controls the local hemodynamics is likely to be larger than the neuronal area of a functional unit, there is a limit in the spatial resolution of those methods based upon hemodynamics such as PET or fMRI. If the match between the area of a functional unit and the coverage of the local vasculature exists, however, the hemodynamic response will represent the area of neuronal activation for that function. This has been demonstrated in whisker barrels in the somatosensory cortex in the rodent brain. Stimulation of a single whisker induces a rCBF increase that is highly localized at the corresponding principal barrel (19). In high-resolution functional MRI of the rat brain, Yang et al (104) showed that a BOLD signal by a single whisker activation is well localized at the whisker-barrel location. Furthermore, the signal appears mostly at layer IV of the cortex. This layer is known to be the site of the input signal processing and with less lateral neural connection than other upper layers. It is $\sim$500 μm deep from the pial surface of the brain and hard to visualize by visible light optical reflectance imaging (22).

In optical imaging of ocular dominance columns in monkey visual cortex (34), the intrinsic signal resulting from hemoglobin absorption was shown to be poorly localized compared to the ocular dominance column structure (especially at the wavelength that represents the blood volume). In order to get the functional map that depicts ocular dominance columns, it was necessary to take the ratio of the two signals, one with left-eye-only and the other with right-eye-only stimulations. This (functional) mapping signal was a fraction of the global signal, the original one-sided signal, which did not show the spatial functional specificity. This distinction of the mapping signal from the global signal has been further demonstrated in the study of spectroscopic imaging of

orientation columns in the cat brain by Malonek et al (63). The distinction comes from the change of the deoxyhemoglobin content associated with the increased metabolic load that should closely represent the area of functional activation. The spectral change caused by the induced CBF increase was not well localized in their experiments.

In the human brain, the size of an ocular dominance column is about 1×1 mm^2 in the cross-section normal to the cortical surface and several to 10 mm long parallel to the surface. Menon et al (68) examined the prospect to observe them by using-high resolution FLASH imaging at 4 Tesla. The size of the imaging voxel was $0.55 \times 0.55 \times 4$ mm^3. Observation of any monocular dominance specificity of these columns requires that their column axes be normal to the imaging slice plane; otherwise, voxels in V1 will be binocularly activated because of the partial-volume effect. When activated areas in V1 were selected in the postprocessing by a histogram analysis of left/right distributions, patchy activation maps could be obtained that were highly specific to the monocular dominance. The size of each area was estimated to be 0.9 mm. The time courses of the activation at these highly monocularly specific areas are shown in Figure 4 for a paradigm of binocular as well as the left and the right eye monocular stimulations in time series. In this global signal plot in time, the functional (ocular dominance) pattern is clearly seen. The signal increase by the monocular activation is as strong as with the binocular activation at these sites and the activation induced by the other eye stimulation is small.

The simplest interpretation of this result is that the hyperoxygenation induced by the activation (CBF increase dominant) is well localized at least in those patchy areas and the signal increase is in the area for the proper eye stimulation and the signal valley in the time course is due to the wrong eye stimulation, not vice versa. This result indicates the spatial resolution of fMRI could be as high as such functional units in ocular dominance columns, although it is necessary to use a difference mapping filter to select those functionally specific activation areas.

FUNCTIONAL MAPPING

Historically, the most compelling argument for the existence of regional specialization of human brain function was first presented by Pierre Paul Broca in the middle 19th century (10). Broca examined a patient who, as a result of a stroke, was unable to speak but was otherwise normal. Based on an autopsy performed subsequent to the patient's death, Broca concluded that the seat of the damage was an egg-size lesion located in the inferior frontal gyrus of the frontal lobe in the left hemisphere; this general area is now commonly referred to as Broca's area although its precise topographical extent remains somewhat

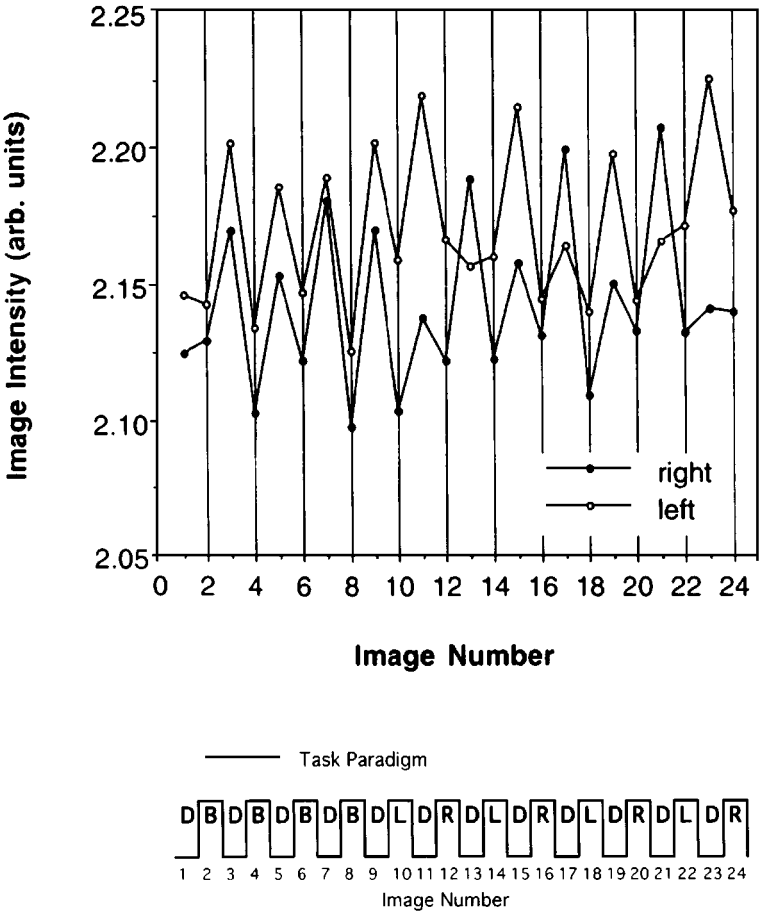

Figure 4 Signal responses to binocular and left-right monocular visual simulation at 4 Tesla. The paradigm is shown at the bottom for 24 periods. *B*, binocular stimulation; *D*, dark; *L*, left-eye stimulation; *R*, right-eye stimulation. In each period of 15 seconds, one FLASH image of 256×256 complex data points with FOV of 14×14 cm^2 and 4 mm slice thickness was measured in sequence (68).

ambiguous. Such lesion studies and later intraoperative mapping efforts with electrodes have been until now the primary source of our current understanding of functional compartmentation in the human brain. The language area first identified by Broca can now be visualized with unprecedented spatial resolution using fMRI in data collection times that last only a few minutes.

As can be ascertained from the previous discussion in this review article, spatial specificity and resolution that can be achieved with fMRI remains one

of the central questions in this new and rapidly evolving field. This question is particularly salient for methods such PET and fMRI, where functional maps are not based on monitoring neuronal activity directly but rather indirectly through the metabolic and hemodynamic response expressed by the cells and vasculature to the presence of increased transmission. With respect to fMRI, this indirect detection raises questions about the contributions of macrovascular inflow effects, macrovascular BOLD effects, and the spatial correspondence between the actual site of neuronal activity and the extent of the metabolic and hemodynamic response. While these issues can be addressed using specific experiments targeted to evaluate them directly, the deleterious consequences of these potential problems can also be evaluated by trying to map functionally distinct structures with well-defined organization and topography in the human brain. Early experiments introducing the methodology had employed such a strategy and demonstrated activation consistent with hemispheric lateralization in brain function. However, detection of functional specialization with respect to hemispheric laterality only reveals the existence of a very course level of spatial specificity, in the domain that can be characterized as several centimeters. On a much finer spatial scale, e.g. millimeter and submillimeter, it is possible to examine activation of small subcortical nuclei and even smaller level neuronal functional organizations such as ocular dominance columns.

The thalamus provides an excellent case for evaluating the question whether structures that are only a few millimeters in size can be accurately mapped by fMRI methodology, and if they can be mapped for tasks that are expected to generate rather weak stimulation. The thalamus contains several distinct, anatomically well defined regions or nuclei. These nuclei serve as a relay point for a remarkably large number of pathways and these various pathways utilize in general separate nuclei. For example, the lateral geniculate nucleus (LGN) is a small, subcentimeter size nucleus located posteriorly and ventrally within the thalamus. The LGN is a primary target of retinal afferents and, in turn, it projects to the primary visual cortex V1. A very strong back projection from V1 to LGN is also present. Therefore, LGN activation must be present during direct visual stimulation because of the retinal input. Because of the back-projection from V1, LGN activation may even be present under circumstances where V1 may be engaged even in the absence of direct photic stimulation, such as during visual mental imagery. Whether LGN activation in the human brain can be robustly detected during photic stimulation and resolved from activation that may be expected in adjacent structures within the thalamus, such as the pulvinar nucleus, was recently examined (14). These studies used high (4 Tesla) magnetic fields that provide advantages in sensitivity and specificity; the study was further extended subsequently to investigate if the V1 and the LGN activation are present together with activation in higher-order visual areas during visual mental imagery tasks. In this effort, the multislice capability of

fMRI to generate a three-dimensional functional map of the whole brain was utilized so as to resolve the LGN from adjacent relevant structures. Figure 5 (see color insert) illustrates images of V1 and bilateral functional activation of the LGN in one participant in three different planes; these planes were extracted from the 3D data set by "reslicing."

In the axial image, the LGN in the two hemispheres are easily identified by their position relative to the optic tract; posteriorly from the optic chiasm, the optic tract runs adjacent to the cerebral peduncle in the midbrain and directly joins the LGN. In the axial image illustrated in Figure 5 (see color insert), the optic tract is seen clearly in both hemispheres near the optic chiasm, anterior to the midbrain. Proceeding posteriorly from the optic chiasm, it appears to merge with the midbrain, and is no longer visualized with clarity because it runs along the cerebral peduncle. Following this curved tract should directly lead to the LGN, which is where the activated loci identified as the LGN are located. In the coronal and parasagittal views, this activated area appears superior to the hippocampal formation as expected for LGN. While the main retinal afferents project to LGN and the geniculostriate projection forms the main pathway for transmission of visual information to the occipital cortex, a secondary pathway exists through the pulvinar nucleus of the thalamus that receives input from the retina and projects reciprocally to the parietal-occipital-temporal association cortex. The pulvinar nucleus in the thalamus, especially the inferior and adjacent lateral parts, must in principle be also activated in photic stimulation experiments; this was observed in these studies (14). The activated pulvinar regions were very close to the LGN neuroanatomically and the two areas could have been difficult to distinguish in most single-slice imaging studies; however, they were well resolved in the three dimensional reconstructed maps.

The specificity inherent in the fMRI data, as illustrated above, has already allowed detailed mapping of various functions in the human brain. One example is the set of studies performed on the visual cortex. Many specialized visual areas, i.e. V1, V2, VP (ventral-posterior), V3, and V4 were recently identified in the human brain for the first time within a short period as compared with laborious invasive animal studies. In fMRI studies, the investigators used the retinotopic organization of these early visual areas (27), but this in itself was not sufficient to identify boundaries of V1 and V2. Retinotopically organized regions of the cortex are divided into two categories when viewed from the cortical surface, those that contain a mirror-image representation of the visual field (e.g. V1), and those that contain a non-mirror-image representation (e.g. V2). Because adjoining areas have a different sign with respect to this representation, they can be and were used to define the borders (83, 92). Figure 6 (see color insert) illustrates images generated based on analysis of retinotopic mapping of the visual field for mirror and non-mirror-image representations where the

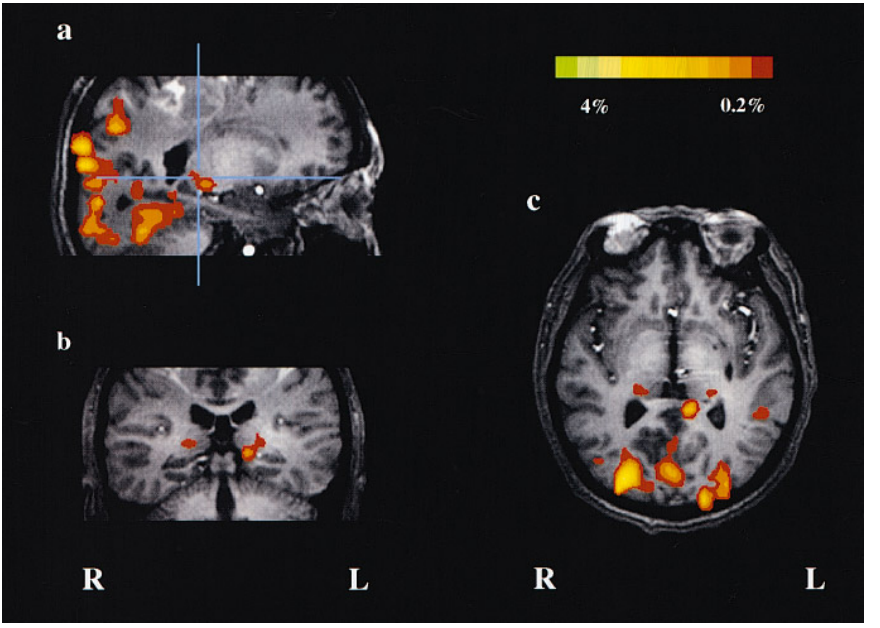

Figure 5 The fMRI maps (in color) superimposed on anatomical images (gray scale) from a single individual during the photic stimulation task illustrating the activation in LGN and V1 areas in the (a) sagittal, (b) coronal and (c) axial image orientations. The cross-point of the two orthogonal lines in (a) identifies the LGN location in this sagittal plane. The two lines define the plane of images in (b) and (c) relative to each other and relative to the sagittal image shown in (a). The LGN activation is shown bilaterally in (b) and (c). (from Chen et al. (14))

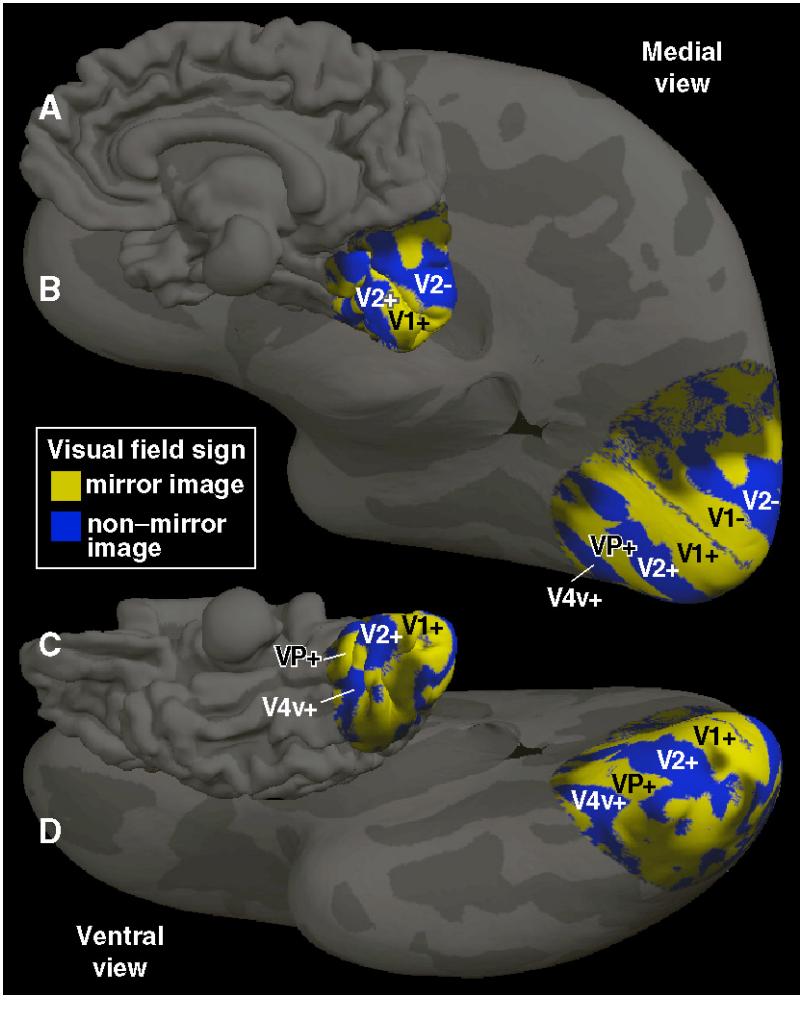

Figure 6 Visual areas V1, V2, V4 and VP in the human visual cortex identified using retinotopic mapping and the mirror versus non-mirror image representation of the visual field. Visual area maps presented either in the normal brain (A and C), or after "unfolding" the various convolutions of the cortical surface so as to generate a flat surface (B and D) for the medial view (A and B) and ventral view (C and D). (from Sereno et al. (83))

boundaries of the early visual areas in the human brain are identified. Here, the advantage of the time-varying input capability of fMRI is used to highlight the neurophysiological characteristics of the activated areas.

SUMMARY AND CURRENT DIRECTIONS

We have reviewed various topics that characterize features of fMRI method and discussed the underlying physiological problem and the relation to neuronal events. The capability of measuring the CBF and BOLD signal on the same individual and within the same paradigm at essentially the same time will soon clarify the quantitative aspect of the BOLD signal. Once the two measurements are well established, then researchers can determine relatively easily the metabolic load associated with functional activation. These physiological parameters may be useful to further characterize the functional activation at a particular site with a particular task in greater detail.

With improvement in the reliability of fMRI measurements, studies with single-trial and short-stimulus presentation paradigms are now possible without the benefit of the multitrial temporal filter usually used in fMRI to improve the statistical reliability of the activation map. Such paradigms can be adjusted to be compatible with those used in other modalities such as MEG. The combination of fMRI and MEG will unite the strength of the two modalities, giving the high temporal resolution to fMRI and the precise locations of multiactivation sites to MEG, so that the uncertainty in solving the inverse problem for source localization is reduced (57). The ultimate goal is to find the functional connectivity among the activation sites at the time scale of neuroinformation transfer.

The field of fMRI is rapidly growing. Its application is already wide in areas of brain research. Further improvement in reliability will turn previously ignored small signal changes, positive or negative, into useful data. This will expand the scope of fMRI to detect more subtle neuronal events such as inhibition. The application of fMRI is expected to expand even further with the easier access to advanced MRI facilities by the brain-science community.

Literature Cited

1. Bandettini P. 1995. *Functional MRI*. PhD thesis. Medical College of Wisconsin
2. Bandettini P, Luh W, Davis T, Van Kylen J, Forster H, et al. 1997. Simultaneous measurement of cerebral perfusion and oxygenation changes during neuronal activation and hypercapnia. *Proc. Annu. Meet. Int. Soc. Magn. Reson. Med., 4th, Vancouver, BC*, p. 740
3. Bandettini PA, Jesmanowicz A, Wong EC, Hyde JS. 1993. Processing strategies for time-course data sets in functional MRI of the human brain. *Magn. Reson. Med.* 30:161–73

4. Bandettini PA, Wong EC, Hinks RS, Tikofsky RS, Hyde JS. 1992. Time course EPI of human brain function during task activation. *Magn. Reson. Med.* 25:390–97
5. Biswal B, DeYoe EA, Hyde JS. 1996. Reduction of physiological fluctuations in fMRI using digital filter. *Magn. Reson. Med.* 35:107–13
6. Biswal B, Hudetz AG, Yetkin FZ, Haughton VM, Hyde JS. 1997. Hypercapnia reversibly suppresses low frequency fluctuations in the human motor cortex during rest using echo planar MRI. *J. Cereb. Blood Flow Metab.* 17:301–8
7. Biswal B, Yetkin FZ, Haughton VM, Hyde JS. 1995. Functional connectivity in the motor cortex of resting human brain using echo-planar MRI. *Magn. Reson. Med.* 34:537–41
8. Boxerman JL, Bandettini PA, Kwong KK, Baker JR, Davis TL, et al. 1995. The intravascular contribution to fMRI signal change: Monte Carlo modeling and diffusion-weighted studies in vivo. *Magn. Reson. Med.* 34:4–10
9. Boxerman JL, Hamberg LM, Rosen BR, Weisskoff RM. 1995. MR contrast due to intravascular magnetic susceptibility perturbations. *Magn. Reson. Med.* 34:555–66
10. Broca P, Brown-Sequard CE. 1855. *Propriétes et fonctions de la moelle épinière: rapport sur quelques experiences de M. Brown-Sequard.* Lu à.la sociéte de biologie le 21 juillet, Bonaventure et Ducessois
11. Buckner RL, Bandettini PA, O'Craven KM, Savoy R, Petersen SE, et al. 1996. Detection of cortical activation during averaged single trials of a cognitive task using functional magnetic resonance imaging. *Proc. Natl. Acad. Sci. USA* 93: 14878–83
12. Buxton RB, Frank LR. 1997. A model for the coupling between cerebral blood flow and oxygen metabolism during neural stimulation. *J. Cereb. Blood Flow Metab.* 17:64–72
13. Buxton RB, Wong EC, Frank LR. 1997. Dynamics of perfusion and deoxyhemoglobin changes during brain activation. *NeuroImage* 5:S32
14. Chen W, Kato T, Zhu XH, Strupp J, Ogawa S, et al. 1997. Mapping of lateral geniculate nucleus activation during visual stimulation in human brain using fMRI. *Magn. Reson. Med.* In press
15. Chien D, Levin DL, Anderson CM. 1994. MR gradient echo imaging of intravascular blood oxygenation: T_2^* determination in the presence of flow. *Magn. Reson. Med.* 32:540–45
16. Cho Z-H, Ro Y-M, Park S-T, Chung S-C. 1996. NMR functional imaging using a tailored RF gradient echo sequence: A true susceptibility measurement technique. *Magn. Reson. Med.* 35:1–5
17. Cohen MS. 1996. Rapid MRI and functional applications. In *Brain Mapping: The Methods*, ed. AW Toga, JC Mazziotta, pp. 223–55. San Diego: Academic
18. Cooper R, Crow HJ, Walter WG, Winter AL. 1966. Regional control of cerebral vascular reactivity and oxygen supply in man. *Brain Res.* 3:174–91
19. Cox SB, Woolsey TA, Rovainen MC. 1993. Localized dynamic changes in cortical blood flow with whisker stimulation corresponds to matched vascular and neuronal architecture of rat barrels. *J. Cereb. Blood Flow Metab.* 13:899–913
20. Davis TL, Kwong KK, Bandettini PA, Weisskoff RM, Rosen BR. 1997. Mapping the dynamics of oxidative metabolism by functional MRI. *Annu. Meet. Int. Soc. Magn. Reson. Med.* 151. Vancouver
21. Detre JA, Leigh JS, Williams DS, Koretsky AP. 1992. Perfusion imaging. *Magn. Reson. Med.* 23:37–45
22. Dowling JL, Henegar MM, Liu D, Rovainen CM, Woolsey TA. 1996. Rapid optical imaging of whisker responses in the rat barrel cortex. *J. Neurosci. Methods* 66:113–22
23. Edelman RE, Siewer B, Darby DG, Thangaraj V, Nobre AC, et al. 1994. Quantitative mapping of cerebral blood flow and functional localization with echo-planar MR imaging and signal targeting with alternating radio frequency. *Radiology* 192:513–20
24. Eichling JO, Raichle ME, Grubb RL, Ter-Pogossian MM. 1974. Evidence of the limitations of water as a freely diffusible tracer in brain of the rhesus monkey. *Circ. Res.* 35:358–64
25. Ellerman J, Garwood M, Henderich K, Hinke R, Hu X, et al. 1994. Functional imaging of the brain by nuclear magnetic resonance. In *NMR in Physiology and Biomedicine*, ed. R Gillies. 137–50. San Diego: Academic
26. Engel SA, Glover GH, Wandell BA. 1997. Retinotopic organization in human visual cortex and the spatial precision of functional MRI. *Cereb. Cort.* 7:181–92
27. Engel SA, Rumelhart DE, Wandell BA, Lee AT, Glover GH, et al. 1994. fMRI of human visual cortex. *Nature* 369:525
28. Fisel CR, Ackerman JL, Buxton RB, Garrido L, Belliveau JW, et al. 1991. MR contrast due to microscopically heterogeneous magnetic susceptibility: numerical

simulations and applications to cerebral physiology. *Magn. Reson. Med.* 17:336–47
29. Fox PT, Raichle ME. 1986. Focal physiological uncoupling of cerebral blood flow and oxidative metabolism during somatosensory stimulation in human subjects. *Proc. Natl. Acad. Sci. USA* 83: 1140–44
30. Fox PT, Raichle ME, Mintun MA, Dence C. 1988. Nonoxidative glucose consumption during focal physiologic neural activity. *Science* 241:462–64
31. Frahm J, Merboldt KD, W H. 1993. Functional MRI of human brain activation at high spatial resolution. *Magn. Reson. Med.* 29:139–44
32. Frahm J, Merboldt KD, Haenicke W, Kleinschmidt A, Boecker H. 1994. Brain or vein-oxygenation or flow? On signal physiology in functional MRI of human brain activation. *NMR Biomed.* 7:45–53
33. Friston KJ. 1996. Statistical parametric mapping and other analyses of functional imaging data. In *Brain Mapping: The methods*, ed. AW Toga, JC Mazziotta, pp. 363–86. San Diego: Academic
34. Frostig RD, Lieke EE, Ts'o DY, Grinvald A. 1990. Cortical functional architecture and local coupling between neuronal activity and the microcirculation revealed by in vivo high-resolution optical imaging of intrinsic signals. *Proc. Natl. Acad. Sci. USA* 87:6082–86
35. Gao J-H, Holland SK, Gore JC. 1988. Nuclear magnetic resonance signal from flowing nuclei in rapid imaging using gradient echo. *Med. Phys.* 15:809–14
36. Gati JS, Menon RS, Ugurbil K, Rutt BK. 1997. Experimental determination of the BOLD field strength dependence in vessels and tissue. *Magn. Reson. Med.* 38:296–302
37. Ginsberg MD, Dietrich WD, Rusto R. 1987. Coupled forebrain increases of local cerebral glucose utilization and blood flow during physiologic stimulation of a somatosensory pathway in the rat: demonstration by double-label autoradiography. *Neurology* 37:11–19
38. Gratton E. 1995. Rapid changes of optical parameters in the human brain during a tapping task. *J. Cogn. Neurosci.* 7:446–56
39. Grinvald A, Frostig RD, Siegel RM, Bartfeld E. 1991. High-resolution optical imaging of functional brain architecture in the awake monkey. *Proc. Natl. Acad. Sci. USA* 88:11559–63
40. Grubb RL, Raichle ME, Eichling JO, Ter-Pogossian MM. 1974. The effects of changes in $PaCO_2$ on cerebral blood volume, blood flow and vascular mean transit time. *Stroke* 5:630–39
41. Gyngell ML, Bock C, Schmitz B, Hoehn-Berlage M, Hossmann K-A. 1996. Variation of functional MRI signal in response to frequency of somatosensory stimulation in a-chloralose anesthetized rats. *Magn. Reson. Med.* 36:13–15
42. Henning J, Janz C, Speck O, Ernst T. 1995. Functional spectroscopy of brain activation following a single light pulse. *Int. J. Imag. Sys. Techol.* 6:203–8
43. Hu X, Le H. 1996. Artifact reduction in EPI with phase-encoded reference scan. *Magn. Reson. Med.* 36:166–71
44. Hu X, Le TH, Parrish T, Erhard P. 1995. Retrospective estimation and correction of physiological fluctuation in functional MRI. *Magn. Reson. Med.* 34:201–12
45. Hu X, Le TH, Ugurbil K. 1997. Evaluation of the early response in fMRI in individual subjects using short stimulus duration. *Magn. Reson. Med.* 37:877–84
46. Hyder F, Chase JR, Gehar KL, Mason GF, Siddeek M, et al. 1996. Increased tricarboxylic acid cycle flux in rat brain during forepaw stimulation detected with 1H[13C]NMR. *Proc. Natl. Acad. Sci. USA* 93:7612–17
47. Jezzard P, Balaban RS. 1995. Correction for geometric distortion in echo planar images from {B_0} field variation. *Magn. Reson. Med.* 34:65–73
48. Jueptner M, Weiller C. 1995. Does measurement of regional cerebral blood flow reflect synaptic activity?—implication for PET and fMRI. *NeuroImage* 2:148–56
49. Kato T. 1997. Monitoring of cerebral multiphasic sustained responses (CMSR) in memory processing using fMRI. *NeuroImage* 5:593
50. Kato T, Kamei A, Takashima S, Ozaki S. 1993. Human visual cortical function during photic stimulation monitored by means of near-infrared spectroscopy. *J. Cereb. Blood Flow Metab.* 13:516–20
51. Kennan R, Zhong J, Gore J. 1994. Intravascular susceptibility contrast mechanisms in tissues. *Magn. Reson. Med.* 31: 9–21
52. Kim S-G. 1995. Quantification of relative blood flow change by flow-sensitive alternating inversion recovery (FAIR) technique: application to functional mapping. *Magn. Reson. Med.* 34:293–301
53. Kim S-G, Tsekos NV. 1997. Perfusion imaging by a flow sensitive alternating inversion recovery (FAIR) technique:

application to functional brain imaging. *Magn. Reson. Med.* 37:425–35
54. Kim S-G, Ugurbil K. 1997. Comparison of blood oxygenation and cerebral blood flow effects in fMRI: estimation of relative oxygen consumption change. *Magn. Reson. Med.* 38:59–65
55. Kim S-G, Ugurbil K. 1997. Functional magnetic resonance imaging of the human brain. *J. Neurosci. Meth.* 74:229–43
56. Kim S-K, Hendrich K, Hu X, Merkle H, Ugurbil K. 1994. Potential pitfalls of functional MRI using conventional gradient-recalled echo techniques. *NMR Biomed.* 7:69–74
57. Kuikka JT, Belliveau JW, Hari R. 1996. Future of functional brain imaging. *Eur. J. Nucl. Med.* 23:737–40
58. Kwong KK, Belliveau JW, Chesler DA, Goldberg IE, Weisskoff RM, et al. 1992. Dynamic magnetic resonance imaging of human brain activity during primary sensory stimulation. *Proc. Natl. Acad. Sci. USA* 89:5675–79
59. Kwong KK, Chesler DA, Weisskoff RM, Donahue KM, Davis TL, et al. 1995. MR perfusion studies with T1-weighted echo planar imaging. *Magn. Reson. Med.* 34:878–87
60. Lai S, Reichenbach JR, Haacke EM. 1996. Commutator filter: a novel technique for the identification of structure's significant susceptibility inhomogeneities and its application to functional MRI. *Magn. Reson. Med.* 36:781–87
61. Latour LL, Hasegawa Y, Formato JE, Fisher M, Sotak CH. 1994. Spreading waves of decreased diffusion coefficient after cortical stimulation in a rat. *Magn. Reson. Med.* 32:189–98
62. Liu H, Chance B, Hielscher AH, Jacques SL, Tittel FK. 1995. Influence of blood vessels on the measurement of hemoglobin oxygenation as determined by time resolved reflectance spectroscopy. *Med. Phys.* 22:1209–17
63. Malonek D, Grinvald A. 1996. Interaction between electrical activity and cortical microcirculation revealed by imaging spectroscopy: implication for functional brain mapping. *Science* 272:551–53
64. Mandeville J, Marota J, Keltner J, Kosovsky B, Burke J, et al. 1996. CBV functional imaging in rat brain using iron oxide agent at steady state concentration. *Proc. Annu. Meet. Int. Soc. Magn. Reson. Med., 3rd, New York*, p. 292
65. Mayer C, Nishimura D, Macovski A. 1992. Fast spiral coronary artery imaging. *Magn. Reson. Med.* 28:202–13
66. McIntosh J, Zhang Y, Kidambi S, Harshbarger T, Mason G, et al. 1996. Echo-time dependence of the functional MRI "fast response". See Ref. 64, p. 284
67. Menon RS, Ogawa S, Hu X, Strupp JP, Anderson P, et al. 1995. BOLD based functional MRI at 4 Tesla includes a capillary bed contribution: Echo planar imaging correlates with previous optical imaging using intrinsic signals. *Magn. Reson. Med.* 33:453–59
68. Menon RS, Ogawa S, Strupp JP, Ugurbil K. 1997. Ocular dominance in human V1 demonstrated by functional magnetic resonance imaging. *J. Neurophysiol.* 77:2780–87
69. Menon RS, Ogawa S, Tank DW, Ugurbil K. 1993. 4 Tesla gradient recalled echo characteristics of photic stimulation-induced signal changes in the human primary visual cortex. *Magn. Reson. Med.* 30:380–86
70. Mitra PP, Ogawa S, Hu X, Ugurbil K. 1997. The nature of spatiotemporal changes in hemodynamics as manifested in functional MRI. *Magn. Reson. Med.* 37:511–18
71. Morita-Tsuzuki Y, Bouskella E, Hardebo JE. 1992. Vasomotion in the rat cerebral microcirculation recorded by laser-Doppler flowmetry. *Acta Physiol. Scand.* 146:431–39
72. Ogawa S, Lee TM, Barrere B. 1993. The sensitivity of magnetic resonance image signals of rat brain to changes in the cerebral venous blood oxygenation. *Magn. Reson. Med.* 29:205–10
73. Ogawa S, Lee TM, Kay AR, Tank DW. 1990. Brain magnetic resonance imaging with contrast dependent on blood oxygenation. *Proc. Natl. Acad. Sci. USA* 87:9868–72
74. Ogawa S, Menon RS, Tank DW, Kim SG, Merkle H, et al. 1993. Functional brain mapping by blood oxygenation level-dependent contrast magnetic resonance imaging. A comparison of signal characteristics with biophysical model. *Biophys. J.* 64:803–12
75. Ogawa S, Tank DW, Menon R, Ellermann JM, Kim S-G, et al. 1992. Intrinsic signal changes accompanying sensory stimulation: functional brain mapping with magnetic resonance imaging. *Proc.Natl. Acad. Sci. USA* 89:5951–55
76. Pellerin L, Magistretti PJ. 1994. Glutamate uptake into astrocytes stimulates arebic glycolysis: a mechanism coupling neuronal activity to glucose utilization. *Proc. Natl. Acad. Sci. USA* 91:10625–29
77. Prichard JW, Rothman DL, Novotny EJ,

Petroff OAC, Kuwabara T, et al. 1991. Lactate rise detected by 1H NMR in human visual cortex during physiologic stimulation. *Proc. Natl. Acad. Sci. USA* 88:5829–31
78. Raichle ME. 1987. Circulatory and metabolic correlates of brain function in normal humans. In *Handbook of Physiology—The Nervous System*, ed. F Plum. 5:643–74. Washington, DC: Am. Physiol. Soc.
79. Richter W, Anderson AP, Georgopoulos AP, Kim S-G. 1997. Sequential activity in human motor areas during delayed cued finger movement task studied by time resolved fMRI. *NeuroReport* 8:1257–61
80. Richter W, Georgopoulos AP, Ugurbil K, Kim S-G. 1997. Time-resolved fMRI of mental rotation. *NeuroReport* 8:3697–3702
81. Roland PE. 1993. *Brain Activation*. New York: Wiley-Liss
82. Rostrup E, Larsson HBW, Toft PB, Garde K, Thomsen C, et al. 1994. Functional MRI of CO_2- induced increase in cerebral perfusion. *NMR Biomed.* 7:29–34
83. Sereno MI, Dale AM, Reppas JB, Kwong KK, Belliveau JW, et al. 1995. Borders of multiple visual areas in humans revealed by functional magnetic resonance imaging. *Science* 268:889–93
84. Shen L, Alexander GE. 1997. Visualization of a sensory-to-motor transformation in motor and premotor cortex. Submitted
85. Shulman RG, Blamire AM, Rothman DL, McCarthy G. 1993. Nuclear magnetic resonance imaging and spectroscopy of human brain function. *Proc. Natl. Acad. Sci. USA* 90:3127
86. Silver A. 1978. Cellular microenvironment in relation to local blood flow. In *Cerebral Vascular Smooth Muscle and its Control*, ed. CF Symposium. 56:49–67. Amsterdam: Elsevier
87. Song A, Wong E, Jesmanowicz A, Tan S, Hyde JS. 1995. Diffusion weighted fMRI at 1.5 T and 3 T. *Annu. Meet. Soc. Magn. Reson. Med.*, Nice, p. 457.
88. Song A, Wong E, Tan S, Hyde J. 1996. Diffusion weighted fMRI at 1.5 T. *Magn. Reson. Med.* 35:155–58
89. Stehling MK, Turner R, Mansfield P. 1991. Echo-Planar imaging: magnetic resonance imaging in a fraction of a second. *Science* 254:43–49
90. Strupp J. 1996. Stimulate, a GUI-based fMRI analysis software package. *NeuroImage* 3:S607
91. Thulborn KR, Waterton JC, Matthews PM, Radda GK. 1982. Oxygenation dependence of the transverse relaxation time of water protons in whole blood at high field. *Biochim. Biophys. Acta* 714:265–70
92. Tootell RGH, Dale AM, Sereno MI, Malach R. 1996. New images from human visual cortex. *Trends Neurosci.* 19:481–89
93. Tsacopoulos M, Magistretti PJ. 1996. Metabolic coupling between glia and neurons. *J. Neuroscience* 16:877–85
94. Turner R, Le Bihan D, Moonen CTW, Frank J. 1991. Echo-planar time course MRI of cat brain oxygenation. *Magn. Reson. Med.* 22:159–66
95. van Gelderen P, de Vleeschouwer MHM, DesPres D, Pekar J, van Zijl PCM, et al. 1994. Water diffusion and acute stroke. *Magn. Reson. Med.* 31:154–63
96. Villringer A, Planck J, Hock C, Schleinkofer L, Dirnagl U. 1993. Near infrared spectroscopy (NIRS): a new tool to study hemodynamic changes during activation of brain function in human adults. *Neurosci. Lett.* 154:101–4
97. Volkow ND, Rosen B, Farde L. 1997. Imaging the living human brain: magnetic resonance imaging and positron emission tomography. *Proc. Natl. Acad. Sci. USA* 94:2787–88
98. Weisskoff RM, Baker J, Belliveau J, Davis TL, Kwong KK, et al. 1993. Power spectrum analysis of functionally-weighted MR data: What's in the noise? *Proc. Annu. Meet. Soc. Magn. Reson. Med. 1st, New York*, p. 7
99. Williams DS, Detre JA, Leigh JS, Koretsky AP. 1992. Magnetic resonance imaging of perfusion using spin inversion of arterial water. *Proc. Natl. Acad. Sci. USA* 89:212–16
100. Woolsey TA, Rovainen CM, Cox SB, Henegar MH, Liang GE, et al. 1996. Neuronal units linked to microvascular modules in cerebral cortex: response elements for imaging the brain. *Cereb. Cort.* 6:647–60
101. Worsley KJ, Marrett S, Neelen P, Vandal AC, Friston KJ. 1996. A unified statistical approach for determining significant signals in images of cerebral activation. *NeuroImage* 4:58–73
102. Yablonskiy DA, Haacke EM. 1994. Theory of NMR signal formation in magnetically inhomogeneous tissue: fast dephasing regime. *Magn. Reson. Med.* 32:749–63
103. Yang QX, Dardzinski BJ, Li S, Eslinger PJ, Smith MB. 1997. Multi-gradient echo with susceptibility inhomogeneity compensation (MGESIC): demonstration of

fMRI in the olfactory cortex at 3.0 T. *Magn. Reson. Med.* 37:331–35
104. Yang X, Hyder F, Shulman RG. 1996. Activation of single whisker barrel in rat brain localized by functional magnetic resonance imaging. *Proc. Natl. Acad. Sci. USA* 93:475–78
105. Ye FQ, Allen PS. 1995. Relaxation enhancement of the transverse magnetization of water protons in paramagnetic suspensions of red cells. *Magn. Reson. Med.* 34:713–20
106. Zhong J, Petroff OAC, Pleban LA, Gore JC, Prichard JW. 1997. Reversible, reproducible reduction of brain water apparent diffusion coefficient by cortical electroshocks. *Magn. Reson. Med* 37:1–6